Broadband optical absorption based on single-sized metal-dielectric-metal plasmonic nanostructures with high-ε'' metals

Wei Wang, Yurui Qu, Kaikai Du, Songang Bai, Jingyi Tian, Meiyan Pan, Hui Ye, Min Qiu, and Qiang Li

Citation: Appl. Phys. Lett. **110**, 101101 (2017); doi: 10.1063/1.4977860
View online: http://dx.doi.org/10.1063/1.4977860
View Table of Contents: http://aip.scitation.org/toc/apl/110/10
Published by the American Institute of Physics

Broadband optical absorption based on single-sized metal-dielectric-metal plasmonic nanostructures with high-ε'' metals

Wei Wang, Yurui Qu, Kaikai Du, Songang Bai, Jingyi Tian, Meiyan Pan, Hui Ye, Min Qiu, and Qiang Li[a)]

State Key Laboratory of Modern Optical Instrumentation, College of Optical Science and Engineering, Zhejiang University, 310027 Hangzhou, China

(Received 21 December 2016; accepted 18 February 2017; published online 6 March 2017)

We propose a broadband, efficient, ultra-thin metal-insulator-metal (MIM) absorber with a simple single-sized disk configuration by utilizing metals with high imaginary part of permittivity (ε''). The physics behind this is that field dissipation is remarkably enhanced in MIM absorbers with high-ε'' metals, significantly extending the absorption bandwidths, which are conventionally limited by magnetic resonances of MIM absorbers with low-ε'' metals. The experimentally demonstrated MIM absorber based on tungsten with high-ε'' yields broadband absorption from visible to near-infrared range (400–1700 nm) with an average measured absorption of 84%. The ultra-thin and single-sized nanostructure with broadband efficient absorption facilitates the scalability to large-area photonic applications. *Published by AIP Publishing*. [http://dx.doi.org/10.1063/1.4977860]

Plasmonic metamaterial absorbers have garnered significant interest due to their unique ability to trap light beyond diffraction limit and potential applications in energy-harvesting and information processing.[1–5] Especially, the broadband absorbers show fascinating applications in photovoltaics and thermophotovoltaics,[6] bolometers,[7] thermal emitters,[8,9] and photodetectors.[10] So far, a lot of strategies have been demonstrated to realize broadband optical absorption with metallic nanostructures, including planar film stacks consisting of alternating metal/dielectric layers,[11,12] anodized aluminum oxide templates filled with metallic nanoparticles,[13] arrays of tapered structures including metal pyramids[14] and convex grooves,[15] and hyperbolic metamaterial arrays.[16] These strategies all show respective merits. However in these schemes, the effective thicknesses of the devices are generally above 400 nm, which are close to or even larger than the optical wavelength.

The metal-insulator-metal (MIM) absorber,[17–22] where metallic nanopatterns and a metallic film are separated by one thin dielectric film, can achieve extreme absorption by concentrating the electromagnetic field in the dielectric gap based on magnetic-resonances. The most prominent feature of the MIM absorber is that its thickness ($\sim$100 nm for absorption in the optical region[17]) is well below the wavelength. However, the absorption based on the magnetic response is accompanied by a comparatively narrow bandwidth ($\sim$200 nm in the near infrared).[17,18] Two methods have been proposed to efficiently extend the bandwidth of the MIM absorber. One is to introduce complicated metallic nanostructures since the resonant wavelength is predominantly dependent on the size of the top metallic nanostructures.[23–26] Another method is to combine the magnetic resonances with the broad Mie resonance of the nanoparticles, which originates from the randomly shaped particles with a large size distribution.[27,28] These methods present advances towards broadband, efficient, ultra-thin MIM absorbers; they yet suffer the problem of either comparatively narrow bandwidth (only covering the visible spectrum) or requiring randomness in nanostructures (such as size, shape, and arrangement variation), which increases fabrication complexity. Besides, compared with noble metals with low stability at high temperature,[29,30] refractory materials with high melting points are much more attractive for the MIM broadband absorber for energy harvesting techniques such as solar thermophotovoltaics. The refractory material-based MIM absorbers with high absorption have been numerically demonstrated from visible to near infrared regions[31] or experimentally at either visible or near infrared spectrum.[32,33] Therefore, it is of vital importance to realize refractory material-based MIM absorbers with simultaneously broadband absorption (covering both visible and near infrared regions) and simple configuration (such as only one size, one shape, and one arrangement for the top nanostructure).

In this paper, we propose a broadband, efficient, ultra-thin MIM absorber with a simple single-sized disk configuration by utilizing metals with high imaginary part of permittivity ($\varepsilon = \varepsilon' + i\varepsilon''$ represents relative permittivity throughout this paper). Much broader absorption bandwidth can be realized with high-ε'' metals compared with conventional low-ε'' metals in the MIM absorber. The physics behind is that field dissipation is significantly enhanced in MIM absorbers with high-ε'' metals, remarkably extending the absorption bandwidth dependent on the conventional magnetic resonances. As a proof-of-concept demonstration, a high-ε'' tungsten based MIM absorber with one consistent disk size is fabricated, which shows an average measured absorption of above 80% from visible to near-infrared range (400–1700 nm). This MIM absorber with high-ε'' metals presents several advantages: (1) broadband and efficient absorption from visible to near-infrared can be realized by combining enhanced field dissipation at both non-magnetic resonances and magnetic resonances; (2) the total thickness of the MIM triple layer is only 215 nm, which is smaller than the light wavelength; (3) although the device demonstrated in this manuscript is still based on e-beam lithography, the simple single-sized

a)E-mail: qiangli@zju.edu.cn

nanostructure configuration can potentially enable cost-effective large-scale fabrication (such as printing lithography[3] and colloidal lithography[21,34]); (4) the high-ε'' metals are usually refractory, paving the way for high-temperature applications. This broadband, efficient, ultra-thin MIM absorber with a simple single-sized disk configuration presents an outstanding candidate for efficient energy-harvesting applications.

The structure of the MIM absorber is illustrated in Fig. 1(a). It consists of three layers: a bottom metal film, an insulator spacer layer, and a top nanostructured metal layer. The thickness of the bottom metal layer is generally larger than its skin depth to prevent leaky transmission. The lossless dielectric layer (Al_2O_3) has a thickness of d (=70 nm). The top structured metallic layer is composed of periodical nanodisks with uniform thickness, radius, and periodicity of t, r, and a, respectively. Numerical simulations are performed by using commercial software COMSOL Multiphysics based on finite element methods. In the simulation, radius r, thickness t, and periodicity a (in both x- and y-directions) of metallic disks are set as 116 nm, 15 nm, and 320 nm, respectively. The refractive index of Al_2O_3 is set as 1.75. Two kinds of metals in terms of the permittivity are considered: one is conventional low-ε'' metal (such as gold (Au)) and the other is high-ε'' metal (such as titanium (Ti), tungsten (W), and nickel (Ni)). The MIM absorbers made of these two kinds of metals are termed as "low-ε'' MIM absorber" and "high-ε'' MIM absorber," respectively. The real parts (ε') and imaginary parts (ε'') of the complex permittivity for the metals considered here are provided in supplementary material Figs. S1 and 1(b), respectively. The complex permittivities of Au, Ti, and Ni are derived from the tabulated data from Johnson.[35,36] The complex permittivity of W is obtained by variable angle spectroscopic ellipsometry in our experiment. At 1060 nm, the ε'' for Ti, W, and Ni is 28.14, 32.58, and 31.42, respectively, far larger than that for Au (3.86).

The absorption spectrum (400–1700 nm) of both the "high-ε'' MIM absorber" and "low-ε'' MIM absorber" with the same geometrical parameters for normal x-polarized excitation is calculated (Fig. 2(a)). From the absorption spectrum, we can see that the high-ε'' MIM absorbers show high absorption from 400 nm to 1700 nm. The average absorption for Ni, Ti, and W MIM absorbers is 82%, 81%, and 84%, respectively. In comparison, low-ε'' (Au) MIM absorbers only show high absorption at obvious resonances: one is at the magnetic resonance (~1400 nm) and the other is at the

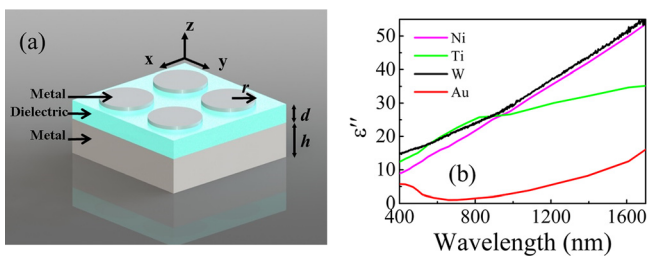

FIG. 1. (a) Three dimensional schematic view of the MIM absorber. (b) Imaginary parts of permittivity for high-ε'' (Ni, Ti and W) and low-ε'' (Au) metals.

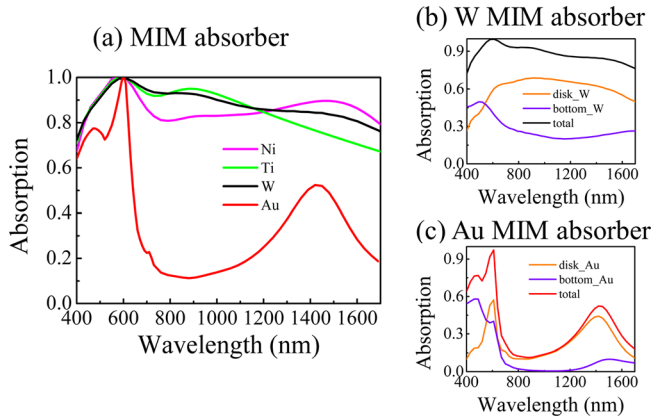

FIG. 2. (a) Comparison of simulated absorption between high-ε'' (Ni, Ti, and W) and low-ε'' (Au) metal based MIM absorbers. (b) and (c) Total absorption, absorption in the top disk and bottom layer for the W MIM absorber and the Au MIM absorber.

anti-reflection resonance (~560 nm). The fractions of the light absorbed in the top metallic disk and the bottom metallic film for the W and Au MIM absorbers are shown in Figs. 2(b) and 2(c).

To investigate the physics behind the remarkable difference in the absorption bandwidth between the high-ε'' and low-ε'' MIM absorbers, electromagnetic field profiles (Figs. 3 and S2) and heat power density (Fig. 4) are further calculated for the Au and W MIM absorbers. The heat power density q is related to the metal loss and the local electric field by $q = \frac{1}{2}\varepsilon_0\omega\varepsilon''|\mathrm{E}|^2$, where ε_0, ω, and $\mathbf{E}$ are vacuum permittivity, angular frequency of the light, and relative permittivity of the metal ($\varepsilon_m = \varepsilon_m' + i\varepsilon_m''$) and local electric field, respectively. Here, three wavelengths with typical resonances are analyzed to unveil the underlying light absorption mechanisms as follows.

(1) At long wavelengths (1690 nm for the W MIM absorber and 1420 nm for the Au MIM absorber), strong magnetic fields are confined in the dielectric gap between the top metal disks and the bottom metal film (Figs. 3(c) and 3(f)), which are typical magnetic resonances contributing

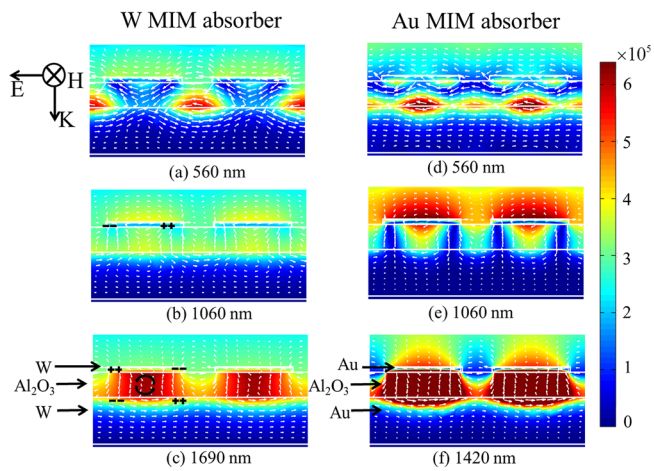

FIG. 3. The magnetic field distributions in the x-z planes bisecting the top nanodisks for the W MIM absorber and Au MIM absorber at typical wavelength. The color contour shows the magnitude of the magnetic field and the vectors denote direction and magnitude of the electric displacement vector.

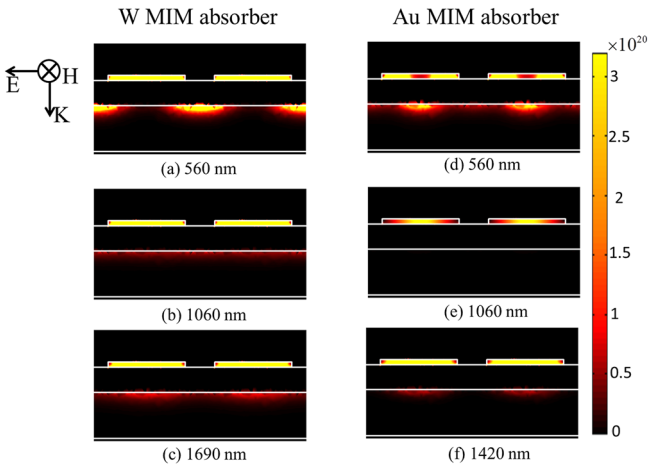

FIG. 4. The heat power density in the x-z planes bisecting the top nanodisks for the W absorber and Au absorber at typical wavelength.

to high absorption (76% and 52% for W and Au MIM absorbers, respectively) (Fig. 2(a)). This magnetic resonance originates from the excited antiparallel currents in the gold disk and the bottom gold layer, forming a closed displacement current loop and bringing about a magnetic moment strongly interacting with the incident magnetic field. For the W MIM absorber, 50% is absorbed by the top metal disk while 26% by the bottom metal film (Fig. 2(b)); while for the Au MIM absorber, 44% is absorbed by the top metal disk and 8% by the bottom metal film (Fig. 2(c)). The heat power density in the top metal disk is much larger than that in the bottom metal film, indicating the role of the bottom metal film as a mirror to reflect light back (Figs. 4(c) and 4(f)).

(2) At short wavelengths (560 nm for both W and Au MIM absorbers), both W and Au MIM absorbers have high absorption (98% and 82%, respectively) (Fig. 2(a)). Strong magnetic fields are confined in the interface between the dielectric and the bottom metallic film, signifying that typical anti-reflection resonances are generated. Conventionally, when an insulator with an optical thickness of one quarter wavelength is coated on a metallic film, the reflected electric field from the metal surface exhibits an opposite phase to the incident electric field and they two negate each other in the thin dielectric film and the reflectance sharply decreases. For the W MIM absorber, the total absorption is 98%, of which 53% is absorbed by the top metal disk and 45% by the bottom metal film (Fig. 2(b)). For the Au MIM absorber, the total absorption is 92%, of which 50% is absorbed by the top metal disk and 42% by the bottom metal film (Fig. 2(c)). The strong absorption in the bottom metal film can also be seen from high heat power density distribution shown in Fig. 4(a).

(3) At medium wavelength (1060 nm for the W MIM absorber and Au MIM absorber), high absorption can be obtained for the W MIM absorber but not for the Au MIM absorber. The absorption is as high as 88% for the W MIM absorber (67% in the top disk and 21% in the bottom film) (Fig. 2(b)) and only 15% in the Au MIM absorber (all in the top disk) (Fig. 2(c)). At this wavelength, it is evident that electric dipoles are excited in the top metallic disks for both the W and Au MIM absorbers (supplementary material Figs. S2(b) and S2(e)). Weak dipoles with opposite orientation can also be identified in the bottom metallic layer; however, they do not strongly couple with the excited dipoles in the top disks and no magnetic resonance can be formed. Although the electric field inside the top metallic disks is weaker in the W MIM absorber than that in the Au MIM absorber (supplementary material Figs. S2(b) and S2(e)), the total absorption in the W MIM absorber is much stronger than that in the Au MIM absorber. This is because ε'' of W (32.58) is much larger than that of Au (3.86) at the wavelength of 1060 nm (Fig. 1(b)), which is the dominating factor for the high absorption in the W MIM absorber even if the electric field is not so strong. For metal with high-ε'' (Ni, Ti, and W), the high field dissipation in metals is further enhanced by the electric dipole resonance. Therefore, high absorption can still be obtained where magnetic resonances and anti-reflection resonances do not exist. Much higher absorption is located in this top metal disk because of the excited dipole resonance (67% in the top metal disk and 21% in the bottom film for the W MIM absorber) (Fig. 2(b)). For metal with low-ε'' (Au absorber), the low field dissipation prevents strong absorption at 1060 nm.

For the low-ε'' absorber, only the magnetic resonances and the anti-reflection resonances contribute to the absorption at resonant wavelength, limiting the available absorption bandwidth. While for the high-ε'' absorber, high field dissipation in the high-ε'' metals induces huge absorption and significantly extends the absorption bandwidth. This field dissipation is further enhanced by the electric dipole resonances since the absorption significantly declines if the top metal disks are replaced by a metal film with the same thickness (Fig. S3). Although the structural parameters of the Au MIM absorber with simple disk nanostructures can be further optimized (changing d from 70 nm to 20 nm) to achieve high absorption at the fundamental magnetic resonance (1630 nm) (Fig. S4), the absorption bandwidth is limited because of the absence of the strong field dissipation at wavelengths where the magnetic resonances and the anti-reflection resonances do not exist.

The low-ε'' (such as gold) MIM absorbers with simple disk nanostructures as the top layer have been well experimentally demonstrated with limited absorption bandwidth.[17,18] As a proof-of-concept demonstration of the high-ε'' absorber, a W MIM absorber with simple single-sized disks as the top layer is fabricated (Figs. 5(a) and 5(b)).

Figure 5(b) depicts the measured and simulated absorption of the W MIM absorber at normal incidence. In comparison, the absorption spectrum of the insulator-metal (IM) double layered film and a single metal layer (M) with the same metal and insulator thickness is provided. The experimental results are in agreement with the simulated results. From 500 nm to 1700 nm, the absorption is maintained above 80%, demonstrating a broad absorption bandwidth. At 790 nm, the measured absorption for the MIM, IM, and M absorbers is 98%, 55%, and 26%, respectively. By adding

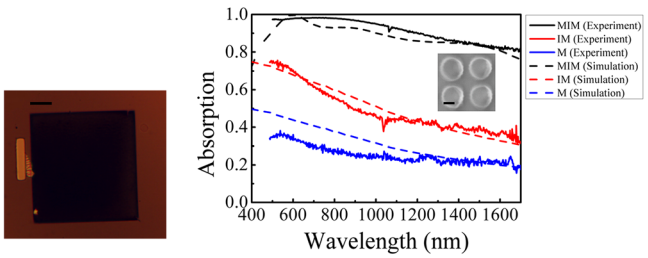

FIG. 5. (a) The optical image of the fabricated 70 μm × 70 μm W MIM absorber. Its scale bar is 15 μm. (b) Comparison of the simulated and experimental absorption spectrum of W (MIM, IM, and M) structure. The inset is a SEM image of the fabricated absorber and its scale bar is 120 nm.

the 15-nm-thick W nanodisks to form a MIM absorber, the absorption gets much higher, demonstrating that the field dissipation in the MIM absorber is enhanced by the resonances. The MIM absorber demonstrates more than twice the absorption of the IM structure at 1700 nm. The smoother experimental absorption spectrum, compared with the simulated spectrum, can be attributed to the additional loss of the nanodisks with rough edges incurred from fabrication, which causes broader resonances. Thus, by combining the magnetic resonances and non-magnetic resonances with high-ε'' metals, broadband, efficient, ultrathin absorption can be realized in the MIM absorber.

In conclusion, we propose a broadband, efficient, and ultrathin MIM absorber with a simple single-sized disk configuration by utilizing high-ε'' metals. The key requirement for the realization of such broadband efficient absorption is identified as the high-ε'' of the metallic materials, which contribute to the high field dissipation and extend the absorption bandwidth dependent on the magnetic resonances and anti-reflection resonances. Compared with the carbon-based absorber, which usually shows large thickness and high emissivity in the middle infrared region, this ultra-thin and simple nanostructure to achieve broadband efficient absorption can facilitate energy-harvesting applications such as solar thermophotovoltaics.

See supplementary material for the procedure of device fabrication, optical simulations, optical characterizations, real part of relative permittivity (for W and Au), electric distribution, and absorption result.

This work was supported by the National Natural Science Foundation of China (Grant Nos. 61425023, 61575177, and 61235007).

[1]T. V. Teperik, F. J. García de Abajo, A. G. Borisov, M. Abdelsalam, P. N. Bartlett, Y. Sugawara, and J. J. Baumberg, Nat. Photonics **2**, 299 (2008).
[2]N. I. Landy, S. Sajuyigbe, J. J. Mock, D. R. Smith, and W. J. Padilla, Phys. Rev. Lett. **100**, 207402 (2008).
[3]S. Han, J.-H. Shin, P.-H. Jung, H. Lee, and B. J. Lee, Adv. Opt. Mater. **4**, 1265 (2016).
[4]D. Shrekenhamer, J. Montoya, S. Krishna, and W. J. Padilla, Adv. Opt. Mater. **1**, 905 (2013).
[5]W. Li, U. Guler, N. Kinsey, G. V. Naik, A. Boltasseva, J. Guan, V. M. Shalaev, and A. V. Kildishev, Adv. Mater. **26**, 7959 (2014).
[6]Z. J. Coppens, I. I. Kravchenko, and J. G. Valentine, Adv. Opt. Mater. **4**, 671 (2016).
[7]K. Du, Q. Li, W. Zhang, Y. Yang, and M. Qiu, IEEE Photonics J. **7**, 1 (2015).
[8]X. Liu, T. Tyler, T. Starr, A. F. Starr, N. M. Jokerst, and W. J. Padilla, Phys. Rev. Lett. **107**, 045901 (2011).
[9]K. Du, Q. Li, Y. Lyu, J. Ding, Y. Lu, Z. Cheng, and M. Qiu, Light: Sci. & Appl. **6**, e16194 (2017).
[10]H. H. Chen, Y. C. Su, W. L. Huang, C. Y. Kuo, W. C. Tian, M. J. Chen, and S. C. Lee, Appl. Phys. Lett. **105**, 023109 (2014).
[11]C. Yang, C. Ji, W. Shen, K.-T. Lee, Y. Zhang, X. Liu, and L. J. Guo, ACS Photonics **3**, 590 (2016).
[12]H. Deng, Z. Li, L. Stan, D. Rosenmann, D. Czaplewski, J. Gao, and X. Yang, Opt. Lett. **40**, 2592 (2015).
[13]L. Zhou, Y. Tan, D. Ji, B. Zhu, P. Zhang, J. Xu, Q. Gan, Z. Yu, and J. Zhu, Sci. Adv. **2**, e1501227 (2016).
[14]E. Rephaeli and S. Fan, Appl. Phys. Lett. **92**, 211107 (2008).
[15]T. Sondergaard, S. M. Novikov, T. Holmgaard, R. L. Eriksen, J. Beermann, Z. Han, K. Pedersen, and S. I. Bozhevolnyi, Nat. Commun. **3**, 969 (2012).
[16]Y. Cui, K. H. Fung, J. Xu, H. Ma, Y. Jin, S. He, and N. X. Fang, Nano. Lett. **12**, 1443 (2012).
[17]J. Hao, J. Wang, X. Liu, W. J. Padilla, L. Zhou, and M. Qiu, Appl. Phys. Lett. **96**, 251104 (2010).
[18]N. Liu, M. Mesch, T. Weiss, M. Hentschel, and H. Giessen, Nano. Lett. **10**, 2342 (2010).
[19]R. Alaee, C. Menzel, U. Huebner, E. Pshenay-Severin, S. Bin Hasan, T. Pertsch, C. Rockstuhl, and F. Lederer, Nano. Lett. **13**, 3482 (2013).
[20]J. A. Bossard, L. Lin, S. Yun, L. Liu, D. H. Werner, and T. S. Mayer, ACS Nano **8**, 1517 (2014).
[21]T. D. Dao, K. Chen, S. Ishii, A. Ohi, T. Nabatame, M. Kitajima, and T. Nagao, ACS Photonics **2**, 964 (2015).
[22]M. J. Rozin, D. A. Rosen, T. J. Dill, and A. R. Tao, Nat. Commun. **6**, 7325 (2015).
[23]G. Tagliabue, H. Eghlidi, and D. Poulikakos, Sci. Rep. **4**, 7181 (2014).
[24]C. W. Cheng, M. N. Abbas, C. W. Chiu, K. T. Lai, M. H. Shih, and Y. C. Chang, Opt. Express **20**, 10376 (2012).
[25]K. Aydin, V. E. Ferry, R. M. Briggs, and H. A. Atwater, Nat. Commun. **2**, 517 (2011).
[26]M. G. Nielsen, A. Pors, O. Albrektsen, and S. I. Bozhevolnyi, Opt. Express **20**, 13311 (2012).
[27]M. K. Hedayati, M. Javaherirahim, B. Mozooni, R. Abdelaziz, A. Tavassolizadeh, V. S. Chakravadhanula, V. Zaporojtchenko, T. Strunkus, F. Faupel, and M. Elbahri, Adv. Mater. **23**, 5410 (2011).
[28]X. Chen, H. Gong, S. Dai, D. Zhao, Y. Yang, Q. Li, and M. Qiu, Opt. Lett. **38**, 2247 (2013).
[29]B. H. Choi, H. H. Lee, S. Jin, S. Chun, and S. H. Kim, Nanotechnology **18**, 075706 (2007).
[30]M. K. Hedayati, A. U. Zillohu, T. Strunskus, F. Faupel, and M. Elbahri, Appl. Phys. Lett. **104**, 041103 (2014).
[31]H. Wang and L. Wang, Opt. Express **21**, A1078 (2013).
[32]F. Ding, J. Dai, Y. Chen, J. Zhu, Y. Jin, and S. I. Bozhevolnyi, Sci. Rep. **6**, 39445 (2016).
[33]W. Li and J. Valentine, Nano. Lett. **14**, 3510 (2014).
[34]M. Rudé, V. Mkhitaryan, A. E. Cetin, T. A. Miller, A. Carrilero, S. Wall, F. J. G. de Abajo, H. Altug, and V. Pruneri, Adv. Opt. Mater. **4**, 1060 (2016).
[35]P. B. Johnson and R. W. Christy, Phys. Rev. B **6**, 4370 (1972).
[36]P. B. Johnson and R. W. Christy, Phys. Rev. B **9**, 5056 (1974).